Optical Materials 75 (2018) 350–356

Contents lists available at ScienceDirect

Optical Materials

journal homepage: www.elsevier.com/locate/optmat

Synthesis of Si/SiO_2 nanoparticles using nanosecond laser ablation of silicate-rich garnet in water

R. Rawat [a], A. Tiwari [a], V.S. Vendamani [b], A.P. Pathak [b], S. Venugopal Rao [c], A. Tripathi [a, *]

[a] Department of Physics, School of Physical Sciences, Sikkim University, 6th mile Samdur, 737102, Sikkim, India
[b] School of Physics, University of Hyderabad, 500046, India
[c] Advanced Center of Research in High Energy Materials (ACRHEM), University of Hyderabad, Hyderabad 500046, India

ARTICLE INFO

Article history:
Received 22 May 2017
Received in revised form
23 October 2017
Accepted 29 October 2017

Keywords:
Laser ablation
Pyrope garnet
Si/SiO_2 nanoparticles

ABSTRACT

During the nanosecond pulsed laser ablation of naturally occurring garnet in water, silicon and silicon dioxide nanoparticles are synthesized. These nanoparticles have an average size of 25 nm and 23 nm when the target is ablated for 20 and 30 min, respectively. The synthesized silicon nanoparticles are crystalline in nature and have cubic structure with 3.0 Å interplanar distance. The effects of laser ablation time on the yield of synthesized nanoparticles in the solution are investigated and it is observed that the optimum ablation time of 20 min is required for the efficient synthesis of silicon nanoparticles while operating at an input pulse energy of 90 mJ. We also report the elemental analysis of the garnet using laser induced breakdown spectroscopy.

© 2017 Elsevier B.V. All rights reserved.

1. Introduction

Eastern Himalaya possesses various types of minerals and rocks. These rocks include different types of gneisses, schists, quartzites, calc-silicates, calc-gneisses, graphite, garnet-kyanite-stauorite, biotite schist, sillimanite, muscovite, garnet etc. [1–3]. The Pyrope garnet belongs to calc-silicate group and is found in abundance in the Himalayan area. Despite being rich in these silicates, neither the elemental composition of these garnets has been investigated precisely nor they have been utilized for the commercial purposes.

Laser-Induced Breakdown spectroscopy (LIBS) [4–7] is often used as an analytical technique for elemental analysis as well as to understand the changes in the physical, chemical and optical properties of the materials. It has been employed on several minerals and rocks samples previously for their compositional analysis [8,9]. In this technique, a short laser pulse is focused on the target surface to create plasma which on cooling emits light of discrete spectral signatures. The light is directed to the detector module for the LIBS analysis. Apart from this, short laser pulse is also employed for the synthesis of nanoparticles (NPs), when the solid target is immersed in liquid media [10–16].

Silicon (Si) and Silicon dioxide (SiO_2) NPs have found potential applications in and as light-emitting devices, catalysis, electronics, thin film substrates, humidity sensors [17–19] and energy sources [20]. There exist several chemical techniques for the synthesis of Si/SiO_2 NPs like sol-gel method [21], microemulsion method [22], chemical vapor deposition (CVD) [23] etc. Unlike these processes, laser ablation of Si-target in the liquid media has been proven an easy and green (no contamination) technique for the synthesis of pure Si nanoparticles [11,12]. However, an alternate to the expensive Si targets remains a challenge for the large scale synthesis of Si NPs using laser ablation techniques.

Here, we report economic, eco-friendly alternative and effective way to synthesize Si/SiO_2 NPs from the naturally occurring silicate-rich garnet rocks. This is the first report on the synthesis of Si/SiO_2 NPs from naturally occurring rock "Pyrope garnet". In this study, we have investigated the elemental composition of the garnet using LIBS technique and report the successful synthesis of Si/SiO_2 NPs using nanosecond laser ablation in deionized water. In addition, the effects of laser ablation time (LAT) on the ablated mass of the synthesized NPs are investigated and the results are discussed.

2. Materials and methods

A rock from the garnet group (as shown in Fig. 1) was collected from Assam Linzey, East Sikkim Gangtok. The garnet was cut into a planar sheet and was sonicated for an hour in deionized water. LIBS experiment was carried out using a Q-switched Nd:YAG laser

* Corresponding author.
E-mail address: ajay_t_2000@yahoo.com (A. Tripathi).

https://doi.org/10.1016/j.optmat.2017.10.045
0925-3467/© 2017 Elsevier B.V. All rights reserved.

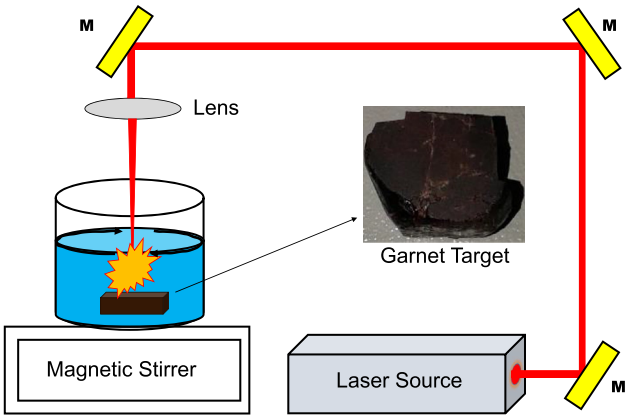

Fig. 1. Experimental setup for laser ablation, where M is 99.9% reflecting mirrors used for laser beam guiding.

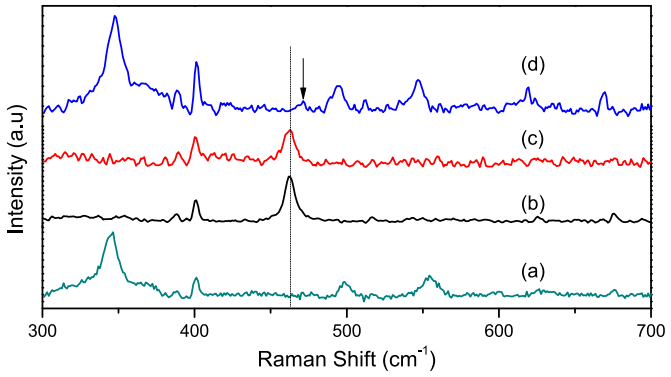

Fig. 3. The Raman spectra of garnet (a) before ablation and after the ablation for (b) 10 min, (c) 20 min and (d) 30 min. The spectra are bore-shifted for clarity.

system (Litton Laser, LPY 707G-10) operating at 1064 nm with 8 ns pulse duration, and a repetition rate of 10 Hz. The LIBS spectra were recorded using Ocean optics USB 2000+ spectrometer coupled with charge coupled device (CCD) in the range of 200–900 nm. For LIBS measurement the garnet target was irradiated with a laser pulse energy of 250 mJ, focused on the surface of the target by using a quartz lens (150 mm focal length). The LIBS setup was further utilized for the synthesis of nanoparticles in deionized water and the experimental setup is shown in Fig. 1. The garnet target was placed at the bottom of a Pyrex cell containing deionized water (18.2 MΩ cm at room temperature) and placed normal to the laser beam (beam waist of 8 mm), which was focused on the garnet surface using the quartz lens. Height of deionized water is 10 mm above the garnet target which was continuously stirred with the help of magnetic stirrer at 800–900 rpm so that the synthesized NPs are properly dispersed in the medium. Formation of large crater is avoided by moving the beaker containing target manually. The formation of large-sized crater(s) is detrimental for ablation efficiency since the input energy is not coupled to the target proficiently. Pulse energy of 90 mJ was used for laser ablation which was kept fixed throughout the experiment. The estimated spot area of laser on the target and the fluence are 4.8×10^{-3}cm^2 and 19 J/cm^2 respectively. The time of ablation was varied from 0 to 30 min in an increment of 10 min. A reasonable step size of 10 min was kept in order to observe changes in the ablated mass in each synthesis step as the ablation rate estimated gravimetrically [24] is found to be low (18 μg/s). Before performing optical and structural analysis, the ablated mass was filtered with Whatman filter paper with pore size of 11 μm.

The absorption spectra of as-synthesized NPs were recorded using Perkin-Elmer Lambda 750 spectrometer. The photoluminescence (PL) spectra of synthesized NPs were recorded by using Perkin-Elmer LS55 spectrometer at the excitation wavelength of 348 nm. Renishaw inVia RM2000 spectrometer with excitation wavelength 785 nm was used to collect the Raman spectra. The size distribution of the NPs has been estimated by using Transmission Electron Microscope (TEM) (Technai, equipped with thermo-ionic electron gun working at 200 kV). The colloidal solution of nanoparticles were drop-casted onto Cu coated TEM grids for TEM characterization.

3. Results and discussion

3.1. Elemental analysis of Pyrope garnet

The elemental analysis of the Pyrope garnet is performed by using the LIBS technique [4,5]. The LIBS spectrum of Pyrope garnet sample is shown in Fig. 2. The spectrum consisted of characteristic atomic lines which are identified using NIST database [25]. The signatures of elements like Mn-I (278.92 nm), Fe-I (373.03 nm), O-I

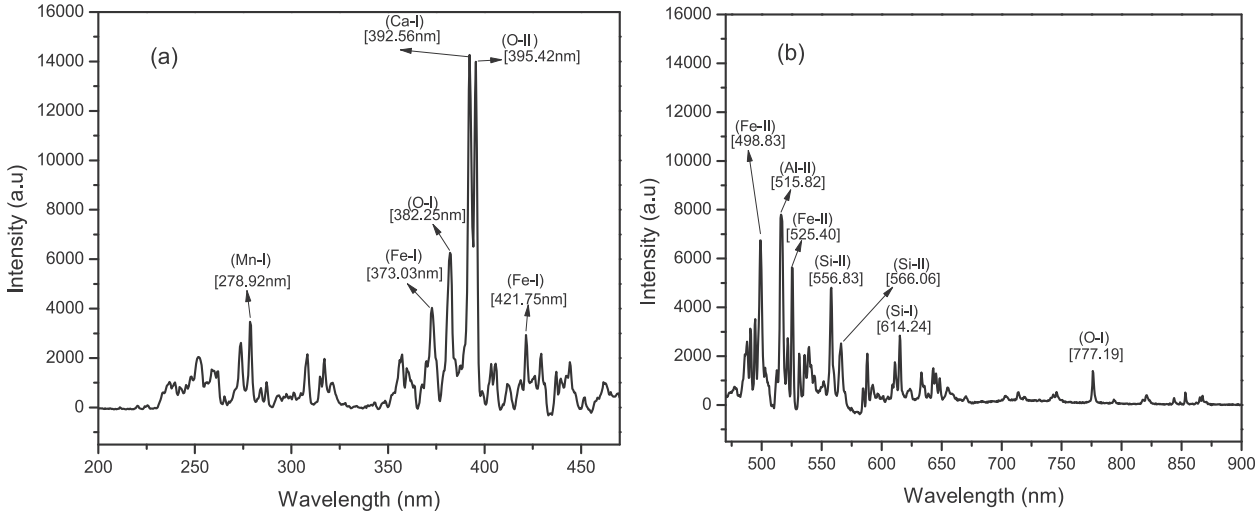

Fig. 2. LIBS spectra of the garnet in the range (a) 200 nm–450 nm, and (b) 450 nm–900 nm.

(382.25 nm), Ca-I (392.56 nm), O-II (395.42 nm), Fe-I (421.75 nm), Fe-II (496. 83 nm), Al-II (515.82 nm), Fe-II (525.40 nm), Si-II (556.83 nm), Si-II (566.06 nm), and O-I (777.18 nm) are noted. From the figure, it can also be seen that Ca-I (392.52 nm), O-II (395.42 nm), O-I (777.19 nm), Fe-I (373.03 nm, 421. 75 nm), Fe-II (496.83 nm, 525.40 nm) and Si-II (556.83 nm, 566.06 nm, 614.24 nm) exhibited more intense peaks as compared to that of other observed elements. The elemental composition is compared with Ruff databse [26] and found to be in agreement with the Pyrope garnet (origin: Warsik, Pakistan).

3.2. Raman and EDS of ablated mass

Fig. 3 shows the Raman spectra of powdered Pyrope garnet along with the ablated mass obtained after the ablation time of 10, 20 and 30 min. In Fig. 3 (a), spectra of powdered Pyrope garnet is shown. Raman shifts at 369 cm^{-1} and 387 cm^{-1} are assigned to rotational mode of R (SiO_4) whereas the shifts between 555 and 630 cm^{-1} and above 675 cm^{-1} are assigned to the internal stretching and bending mode of Si-O in tetrahedral SiO_4 respectively. The observed Raman modes of Pyrope garnet are in line with the previously assigned vibrational modes of Pyrope garnet [27–29]. Upon laser ablation of Pyrope garnet (Fig. 3(b and c), the Raman mode at 462.2 ± 0.1 cm^{-1} is observed whose position remains unchanged with the ablation time of 10 min and 20 min and their full width at half maxima (FWHM) is found to be 7.7 ± 0.2 cm^{-1} and 8.5 ± 0.3 cm^{-1} respectively. As reported by Alessi et al., 2013 [30], the observed Raman mode at 462 cm^{-1} can be attributed to the R line of SiO_2 nanoparticles. Upon laser ablation of 30 min, this mode (462 cm^{-1}) shifts towards the higher wavenumber (469 cm^{-1}) as indicated by an arrow in Fig. 3(d) and has FWHM of 8.9 ± 0.8 cm^{-1}. This shifts towards the higher wavenumber could be attributed to the smaller size SiO_2 NPs upon prolonged ablation. Energy dispersive X-ray spectroscopy (EDS) of laser ablated garnet particulates in water has also been performed. It has been observed that in addition to O (wt.% = 64.67), Si(wt.% = 10.52), Ca (wt.% = 14.28) and trace elements like Mg (wt.% = 6.92) and Al (wt.% = 3.61) are present in the ablated garnet solution.

For the ns pulse with a high fluence, ablation of the metal target occurs due to plasma formation and eventually, the constituents of plasma forms nanoparticles [31]. Therefore, it is expected to have mixtures of NPs of Mg, Al and Si during the ablation of the Pyrope garnet. However, only Si/SiO_2 NPs are observed in the present case. Despite increasing the ablation energy from 90 mJ to 120 mJ, the traces of Mg, Al or their oxides NPs remain unseen (see Fig. S.1 in supplementary information). This may be attributed to the presence of Si, Al, and Mg oxides in the garnet where the energy provided is not enough to dissociate the bonds to form individual elements. It is demonstrated by the following calculation: Pyrope, chemical formula $Mg_3Al_2(SiO_4)_3$ (as shown in Fig. 4(a)) [32], is combination of 3 MgO (dissociation energy of 3×394 kJ/mol) + Al_2O_3 (dissociation energy of 1675 kJ/mol) + 3 SiO_2 (dissociation energy of 3×798 kJ/mol). Therefore, the energy required to break bonds of 1 mol of Pyrope would be 5×10^3 kJ/mol. The density and molecular weight of Pyrope is 3.74 g/cm^3 and 403.13 g respectively. For 1064 nm laser, ablation depth would be very small and the energy dissipation may be limited to the surface only (as shown in Fig. 4(b)). This means that hardly 0.01 mol are exposed to 19 J upon laser ablation. The energy required to break the bonds of 0.01 mol would be approximately 50 kJ which is beyond the 19 J limit. In the presented work, ablation process is purely thermal where the process of melting and vapourization of the target is involved. Pulse width of 8 ns is enough to allow the melted material to reach liquid-vapor equilibrium [33] and the formation of nanodroplets will be preferred over the plasma. Assuming congruent melting of Pyrope upon laser ablation into the immiscible liquids of Al, Mg and Si oxides, SiO_2, being less dense and more volatile [34], will have more participation in the nanodroplet formation as compare to Mg and Al oxides. In one of the recent reports wherein Mica sheet was ablated with 40 fs laser pulse with waist size of ≈ 30 μm and the input energy of 100 μJ [35], the formation of Mg NPs and there derivatives has been reported. The fluence of the laser pulses used there was $>10^2$ kJ/cm^2, which is probably sufficient to dissociate the bonds involved. The pulse width (≈ 40 fs) being far less than electron phonon coupling time [36], thermal effect is minimal and ablation will involve the process of sublimation. The enthalpy of vapourization of Mg being less, participation of Mg will be more as compared to other constituents. In addition to Mg, Al, O and Si we have seen the presence of Ca in the sample which might be due to the presence of natural contaminants on surface like traces of andradite garnet. Despite the wt. % of calcium is more than that of Si, the formation of Ca-NPs is ruled out due to the high reactivity of Ca ions [37] and the absence of capping agents in the solution. However, further detailed experiments with different composition of the target and specifically, different focal condition are being planned to completely understand and explain the phenomenon observed in the present

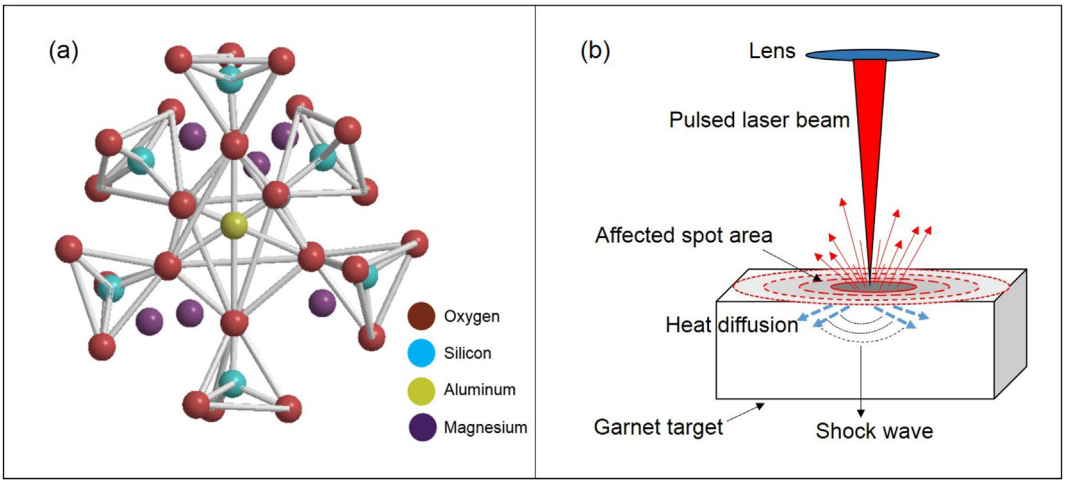

Fig. 4. (a) Crystal structure of Pyrope garnet showing the surface contain most of the Silicon and Oxygen, (b) Nanosecond pulse laser interaction with the garnet target.

experiment.

3.3. TEM analysis

Fig. 5(a and b) show TEM micrographs of colloidal Si/SiO_2 NPs obtained upon the laser ablation of the garnet target for 20 and 30 min respectively. Their respective size distributions are shown in Fig. 5 (c and d). The NPs are nearly spherical in shape and have wide size distribution in the range 7 nm–75 nm (average NPs size = 25 nm) when the garnet target is ablated for 20 min. Likewise with increase in ablation time to 30 min, NPs with an average size of 23 nm are obtained with similar size distribution ranging between 12 nm and 62 nm. These results demonstrate that the size of Si/SiO_2 NPs does not change significantly with increase in laser ablation time from 20 to 30 min. It is evident that the colloidal solution contains significant amount of large sized particulates (100 nm- 500 nm) on which the smaller sized NPs are been adsorbed/deposited (additional images are provided in Supplementary Figure S.2). These large sized particulates may be the unvaporized melts of garnet consisting of Si, Al, Mg and their oxides (as observed from EDS data) which have probably re-solidified and are deposited on the target in the form of debris [38]. The debris is in general amorphous in nature (because of slow cooling) and are weakly attached to the target. It can be further ablated with the subsequent laser pulses and/or is stirred away from the interaction zone by the whirling liquid [39]. NPs present in the solution can get adsorbed on debris and may interact with its local environment during the ablation time. However, the optical measurements, as discussed in the latter section, show absence of any interactions between the NPs and the debris.

Fig. 6 (a and b) show HRTEM image of single NP obtained when the garnet was ablated for 20 and 30 min respectively. The crystalline lattice plane with an inter-planar distance of 0.30 (±0.01) nm is observed corresponding to the [111] lattice plane of Si NPs [12,40–42]. It is evident that with increase in the laser ablation time the crystalline nature of the as-synthesized Si NPs remains

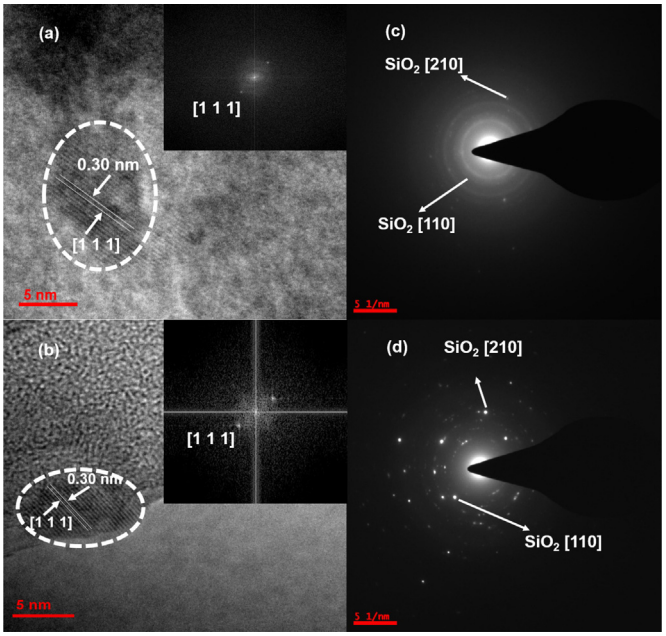

Fig. 6. HRTEM image of Si NPs obtained when the garnet was ablated for (a) 20 min and (b) 30 min showing [111] crystal plane, and the inset shows its fast Fourier transform. (c) and (d) show SAED patterns of colloidal Si/SiO_2 NPs when the garnet was ablated for 20 and 30 min respectively.

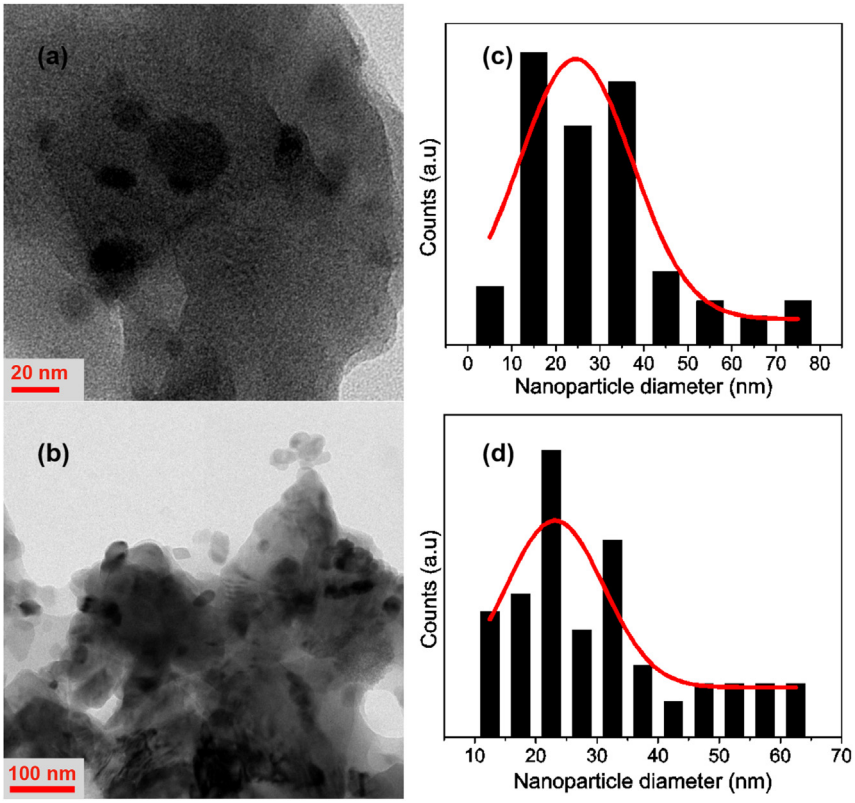

Fig. 5. TEM images of the Si/SiO_2 NPs synthesized from the garnet for ablation time (a) 20 min and (b) 30 min whose size distribution is given in (c) and (d) respectively.

unchanged [11,12]. Fig. 6 (c and d) show SAED patterns of the colloidal Si/SiO_2 NPs obtained when the garnet was ablated for 20 and 30 min. The SAED pattern reveals the presence of [111], [220], [311] and [320] cubic planes of Si NPs for which the inter-planar distances are found to be around 0.300 nm, 0.185 nm, 0.156 nm and 0.145 nm respectively. In addition, the lattice planes [210] and [110] of cubic SiO_2 NPs are also observed with respective inter-planar distances 0.156 nm and 0.244 nm [43].

3.4. Effect of laser ablation time on the optical properties of Si/SiO_2 NPs

Fig. 7 (a, b and c) show the UV–Visible absorption spectra of colloidal NPs synthesized from the laser ablation of the garnet and having ablation time of 10 min, 20 min and 30 min respectively. In inset of Fig. 7 the absorption spectrum of the sample ablated for 10 min was fitted with two peaks at 256 ± 3 nm and 346 ± 3 nm which are attributed to the presence of SiO_2 NPs [18,44–46] and Si NPs [40,47–50], respectively. The respective linewidths of 256 nm and 346 nm peaks are found to be 79 ± 6 nm and 57 ± 3 nm. Upon prolonged ablation of garnet in water, the observed peak positions and their linewidths remain unaltered. This can be attributed to the presence of homogeneously distributed Si/SiO_2 NPs in the solution.

Fig. 8(a, b and c) show the PL spectra of the sample ablated for 10 min, 20 min and 30 min respectively. In all three cases emission is broad (ranges from 360 nm to 550 nm) and having maximum PL intensity around 430 nm. The broad emission is in the conformity with observed wide size distribution (7 nm-75 nm) of the synthesized NPs. In inset of Fig. 8, PL spectrum of the sample ablated for 10 min is shown which can be fitted with three Gaussian peaks P1 (centered at 415.6 ± 0.2 nm), P2 (centered at 433 ± 1 nm) and P3 (centered at 464 ± 2 nm). The linewidths of the de-convoluted peaks P1, P2 and P3 are found to be 23.3 ± 0.8 nm, 38 ± 1 nm and 78 ± 1 nm respectively. With change in the ablation time, no significant change in the peak positions is observed. The origin of peaks P1 and P2 in the blue region can be attributed to the quantum size confinement effect or to the presence of defects state [51]. Yang et al. [52,53] in his work, where Si NPs were synthesized by ablating Si target in water environment, have reported the presence of two distinguished PL peaks at 415 nm and 435 nm. These peaks are

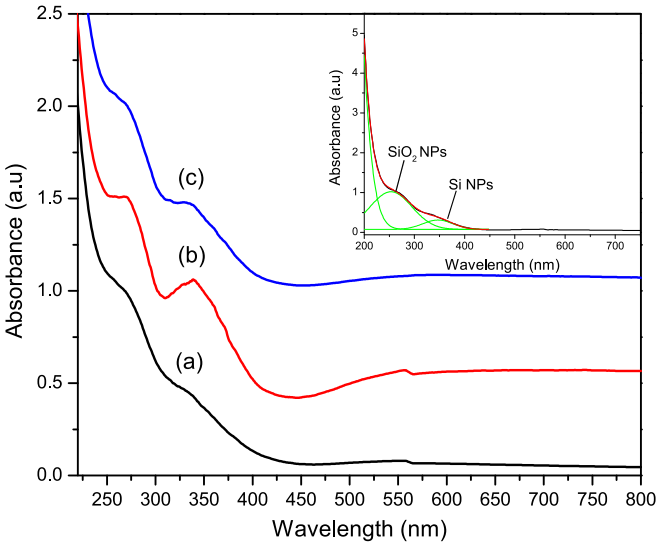

Fig. 7. UV–Visible absorption spectra of Si/SiO_2 NPs synthesized from the garnet while ablating for (a) 10 min (b) 20 min and (c) 30 min. Inset corresponds the curve fitting of the absorption spectrum of Si/SiO_2 NPs obtained from 10 min ablation of the garnet.

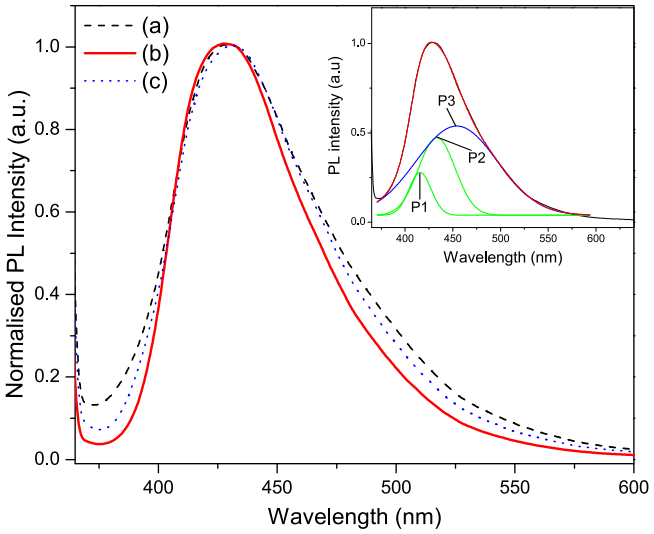

Fig. 8. PL spectra of Si/SiO_2 NPs synthesized from the garnet while ablating for (a) 10 min (dash line) (b) 20 min (Solid dash line) and (c) 30 min (dotted line). Inset correspond to the curve fitting of the PL spectrum of Si/SiO_2 NPs obtained from 10 min ablation of the garnet.

ascribed to the excitons which tend to transfer and recombine at the interface area between Si NPs and surrounding SiO_x ($0 < x < 2$) layers giving rise to strong blue PL. The separation between the two peaks is attributed to the presence of stretching vibrational mode of Si-O-Si. In our case separation of these peaks is not been observed which might be due the synthesis of bigger size NPs as compare to them. The formation of SiO_x layer is because of the replacement of dangling bonds and the dimers surrounding the Si NPs with OH termination, which is present because of the fragmentation of the water molecules. Si-OH bond formed will eventually condensed to form oxides layer [54]. In addition to P1 and P2 the broad peak P3 that extend from blue to green region is also been observed. Commonly the blue green PL emission is attributed to the F-band transitions in SiO_2 nanoparticles. The emission is mainly attributed to Si-OH group which are adsorbed on the Si or SiO_2 nanostructure while being immersed in water [55,56]. As the observed absorption and PL spectra of these NPs are analogous to those of Si/SiO2 NPs, we believe that the synthesized NPs, despite being adsorbed/deposited on the debris, do not have notable interaction with its environment. This could be because the NPs are adsorbed only on the surface of the debris with weak adhesive force.

The area under any spectral peak is attributed to the measure of number of particles involved in that absorption/emission [57]. In order to understand the effects of ablation time on the yield of Si/SiO_2 NPs, we have investigated the area of the peaks observed in UV–Visible and PL spectra. As mentioned earlier, the absorption peaks at 346 nm and 256 nm are attributed to Si NPs and SiO_2 NPs respectively whereas PL peaks P1 and P2 are attributed to Si NPs and, P3 peak is attributed to SiO_2 NPs.

Fig. 9 (a and b) show the relative yield (in percentage) of Si NPs and SiO_2 NPs as a function of laser ablation time as obtained from the absorption and PL measurements respectively. In Fig. 9(a), with increases in ablation time from 10 to 20 min, Si NPs yield increases from 16 (3)% to 30 (5)% whereas for SiO_2 NPs, the yield drops from 84 (19)% to 70 (12)%. Upon further increase in the ablation time to 30 min, Si NPs yield drops to 19 (4)% whereas that of SiO_2 NPs increases to 81 (19)%. In general, increase in ablation time increases the yield of the nanoparticles [58]. However, the observed decrease in the yield of Si NPs for 20–30 min ablation time is attributed to the formation of the particles cloud which shields the actual laser

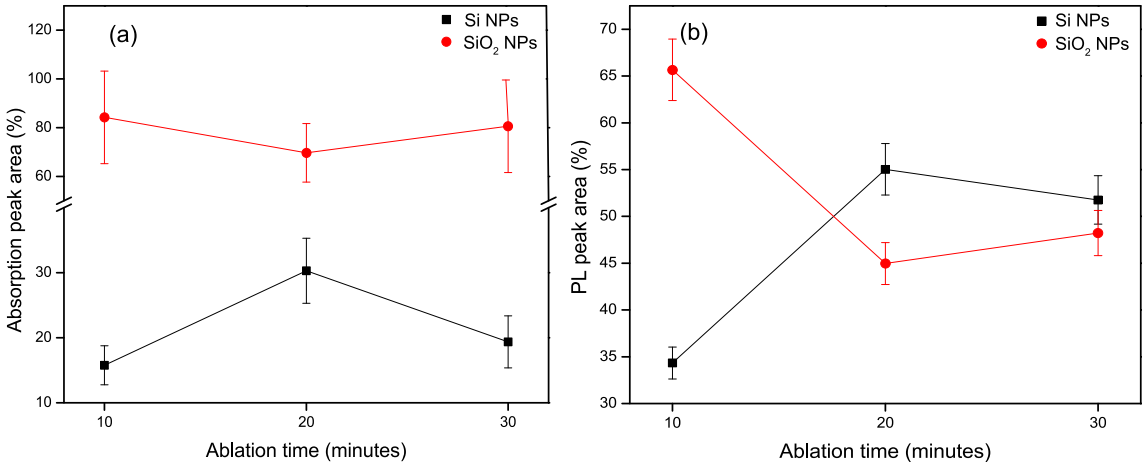

Fig. 9. Area percentage obtained from (a) UV–Visible absorption and (b) PL spectra of Si/SiO_2 NPs as a function of laser ablation time.

power reaching to the target surface [58,59]. On the other hand, when the garnet is being exposed to the laser for longer time, the generation of high temperature in the vicinity results in oxidation of Si to SiO_2 NPs [12,60,61]. We did not extended the ablation time beyond 30 min because after that, the concentration of SiO_2 NPs were dominant over that of Si NPs. Similar trend in the yield percentage of Si and SiO_2 NPs is observed from the PL measurement as shown in Fig. 9(b).

4. Conclusions

In summary, successful synthesis of Si/SiO_2 NPs is achieved using laser ablation of naturally occurring Pyrope garnet rock. These NPs have cubic structure with an inter-planar distance of 3.0 Åand are nearly spherical in shape with wide size distribution between 7 nm and 75 nm. While exciting the samples at 348 nm, a strong blue luminescence is observed near 430 nm. The observed PL spectrum can be fitted with three Gaussians peaks centered at 420, 433 and 454 nm. The origin of peaks 420 and 433 nm has been attributed to the near interface traps at Si-NPs having a coat of SiO_x whereas 454 nm peak is assigned to SiO_2 NPs. The presence of SiO_2 NPs in all the samples has been further confirmed by the appearance of Raman peak at 462.2 cm^{-1} which has been ascribed to the R line of SiO_2 NPs. In addition, time dependent ablation of garnet samples and their optical spectra are also examined revealing that the synthesis of Si NPs is favored over that of SiO_2 NPs when the sample is ablated for 20 min in water. Unlike pure targets, the ablation mechanism is not straightforward and may depend on the crystal structure, binding energy, bond strength etc. other than input laser and physical parameters. A detailed study may be required to understand the synthesis process of a selective nanoparticle from the complex composition. To the best of our knowledge, this is the first report of the synthesis of Si NPs by the laser ablation of naturally occurring silicate rocks. This procedure has the potential to be scaled up as low cost method towards the mass synthesis of silicon and other novel NPs for various applications such as electronics and optoelectronics.

Acknowledgement

RR acknowledges the financial support from RGNF-UGC, Government of India. SVR thanks funding from DRDO, India and UPE-II, University of Hyderabad. VSV thanks CSIR for RA in CSIR emeritus Scientist project awarded to APP.

Appendix A. Supplementary data

Supplementary data related to this article can be found at https://doi.org/10.1016/j.optmat.2017.10.045.

References

[1] J. Ganguly, S. Dasgupta, W. Cheng, S. Neogi, Exhumation history of a section of the Sikkim Himalayas, India: records in the metamorphic mineral equilibria and compositional zoning of garnet, Earth Planet. Sci. Lett. 183 (3) (2000) 471–486.
[2] M. Ghose, Indian small-scale mining with special emphasis on environmental management, J. Clean. Prod. 11 (2) (2003) 159–165.
[3] S. Neogi, S. Dasgupta, M. Fukuoka, High P–T polymetamorphism, dehydration melting, and generation of migmatites and granites in the Higher Himalayan Crystalline Complex, Sikkim, India, J. Petrol 39 (1) (1998) 61–99.
[4] A.W. Miziolek, V. Palleschi, I. Schechter, Laser Induced Breakdown Spectroscopy, Cambridge University Press, 2006.
[5] J.D. Winefordner, I.B. Gornushkin, T. Correll, E. Gibb, B.W. Smith, N. Omenetto, Comparing several atomic spectrometric methods to the super stars: special emphasis on laser induced breakdown spectrometry, LIBS, a future super star, J. Anal. At. Spectrom. 19 (9) (2004) 1061–1083.
[6] T. Tjärnhage, P.-Å. Gradmark, A. Larsson, A. Mohammed, L. Landström, E. Sagerfors, P. Jonsson, F. Kullander, M. Andersson, Development of a laser-induced breakdown spectroscopy instrument for detection and classification of single-particle aerosols in real-time, Opt. Commun. 296 (2013) 106–108.
[7] Y. Yu, W. Zhou, X. Su, Detection of Cu in solution with double pulse laser-induced breakdown spectroscopy, Opt. Commun. 333 (2014) 62–66.
[8] D.M. Díaz Pace, N.A. Gabriele, M. Garcimuño, C.A. D'Angelo, G. Bertuccelli, D. Bertuccelli, Analysis of minerals and rocks by laser-induced breakdown spectroscopy, Spectrosc. Lett. 44 (6) (2011) 399–411.
[9] M.A. Gondal, M.M. Nasr, Z. Ahmed, Z.H. Yamani, Determination of trace elements in volcanic rock samples collected from cenozoic lava eruption sites using LIBS, J. Environ. Sci. Health, Part A Toxic/Hazard. Subst. Environ. Eng. 44 (5) (2009) 528–535.
[10] D. Zhang, B. Gokce, S. Barcikowski, Laser synthesis and processing of colloids: fundamentals and applications, Chem. Rev. 117 (5) (2017) 3990–4103.
[11] R. Intartaglia, K. Bagga, F. Brandi, Study on the productivity of silicon nanoparticles by picosecond laser ablation in water: towards gram per hour yield, Opt. Express 22 (3) (2014) 3117–3127.
[12] R. Intartaglia, K. Bagga, F. Brandi, G. Das, A. Genovese, E. Di Fabrizio, A. Diaspro, Optical properties of femtosecond laser-synthesized silicon nanoparticles in deionized water, J. Phys. Chem. C 115 (12) (2011) 5102–5107.
[13] P. Vasa, R. Sharma, M. Singh, A.K. Dharmadhikari, J.A. Dharmadhikari, D. Mathur, Generation of stable colloidal gold nanoparticles by ultrashort laser-induced melting and fragmentation, Mater. Res. Express 1 (3) (2014) 035028.
[14] G. Kurumurthy, K.S. Alee, D.N. Rao, Photoluminescence studies of Si/SiO_2 nanoparticles synthesized with different laser irradiation wavelengths of nanosecond pulse duration, Opt. Commun. 282 (17) (2009) 3509–3512.
[15] G. Fan, S. Ren, S. Qu, Q. Wang, R. Gao, M. Han, Stability and nonlinear optical properties of Cu nanoparticles prepared by femtosecond laser ablation of Cu target in alcohol and water, Opt. Commun. 330 (2014) 122–130.
[16] S. Chen, T. Wang, Y. Li, J. Liang, D. Wellburn, C. Liu, The structure and magnetic properties of Ag–Ni–SiO2 nano-composite particles produced by pulsed laser control synthesis, Mater. Res. Express 2 (1) (2015) 015018.

[17] H. Giesche, Synthesis of monodispersed silica powders II. Controlled growth reaction and continuous production process, J. Eur. Ceram. Soc. 14 (3) (1994) 205–214.
[18] R. Stanley, A.S. Nesaraj, Effect of surfactants on the wet chemical synthesis of silica nanoparticles, Int. J. Appl. Sci. Eng. 12 (1) (2014) 9–21.
[19] K. Tadanaga, K. Morita, K. Mori, M. Tatsumisago, Synthesis of monodispersed silica nanoparticles with high concentration by the Stöber process, J. Sol-Gel Sci. Technol. 68 (2) (2013) 341–345.
[20] M. Stupca, M. Alsalhi, T. Al Saud, A. Almuhanna, M. Nayfeh, Enhancement of polycrystalline silicon solar cells using ultrathin films of silicon nanoparticle, Appl. Phys. Lett. 91 (6) (2007) 063107.
[21] W. Stöber, A. Fink, E. Bohn, Controlled growth of monodisperse silica spheres in the micron size range, J. Colloid Interface Sci. 26 (1) (1968) 62–69.
[22] I. Abarkan, T. Doussineau, M. Smaihi, Tailored macro/microstructural properties of colloidal silica nanoparticles via microemulsion preparation, Polyhedron 25 (8) (2006) 1763–1770.
[23] K. Nakaso, B. Han, K. Ahn, M. Choi, K. Okuyama, Synthesis of non-agglomerated nanoparticles by an electrospray assisted chemical vapor deposition (ES-CVD) method, J. Aerosol Sci. 34 (7) (2003) 869–881.
[24] P. Chewchinda, O. Odawara, H. Wada, The effect of energy density on yield of silicon nanoparticles prepared by pulsed laser ablation in liquid, Appl. Phys. A 117 (1) (2014) 131–135.
[25] J.E. Sansonetti, W.C. Martin, Handbook of basic atomic spectroscopic data, J. Phys. Chem. Ref. Data 34 (4) (2005) 1559–2259. URL, http://physics.nist.gov/PhysRefData/ASD.
[26] A. Hofmeister, A. Chopelas, Vibrational spectroscopy of end-member silicate garnets, Phys. Chem. Min. 17 (6) (1991) 503–526.
[27] Z. Liu, W. Du, T. Shinmei, S. Gréaux, C. Zhou, T. Arimoto, T. Kunimoto, T. Irifune, Garnets in the majorite–pyrope system: symmetry, lattice microstrain, and order–disorder of cations, Phys. Chem. Min. (2016) 1–9.
[28] L. Maschio, B. Kirtman, S. Salustro, C.M. Zicovich-Wilson, R. Orlando, R. Dovesi, Raman spectrum of pyrope garnet. a quantum mechanical simulation of frequencies, intensities, and isotope shifts, J. Phys. Chem. A 117 (45) (2013) 11464–11471.
[29] B. Kolesov, C. Geiger, Raman spectra of silicate garnets, Phys. Chem. Min. 25 (2) (1998) 142–151.
[30] A. Alessi, S. Agnello, G. Buscarino, F. Gelardi, Structural properties of core and surface of silica nanoparticles investigated by raman spectroscopy, J. Raman Spectrosc. 44 (6) (2013) 810–816.
[31] J. Xiao, P. Liu, C. Wang, G. Yang, External field-assisted laser ablation in liquid: an efficient strategy for nanocrystal synthesis and nanostructure assembly, Prog. Mater. Sci.
[32] F. Pascale, C.M. Zicovich-Wilson, R. Orlando, C. Roetti, P. Ugliengo, R. Dovesi, Vibration frequencies of mg3al2si3o12 pyrope. an ab initio study with the crystal code, J. Phys. Chem. B 109 (13) (2005) 6146–6152.
[33] P. Lorazo, L.J. Lewis, M. Meunier, Thermodynamic pathways to melting, ablation, and solidification in absorbing solids under pulsed laser irradiation, Phys. Rev. B 73 (13) (2006) 134108.
[34] A. Hashimoto, Evaporation metamorphism in the early solar nebulaevaporation experiments on the melt feo-mgo-sio2-cao-al2o3 and chemical fractionations of primitive materials, Geochem. J. 17 (3) (1983) 111–145.
[35] V. Vendamani, A. Tripathi, A.P. Pathak, S.V. Rao, A. Tiwari, Laser ablation of natural micas: synthesis of mgo and mg (oh) 2 nanoparticles and nanochains, Mater. Lett. 192 (2017) 29–32.
[36] B.N. Chichkov, C. Momma, S. Nolte, F. Von Alvensleben, A. Tünnermann, Femtosecond, picosecond and nanosecond laser ablation of solids, Appl. Phys. A 63 (2) (1996) 109–115.
[37] U. Sanyal, R. Datta, B.R. Jagirdar, Colloidal calcium nanoparticles: digestive ripening in the presence of a capping agent and coalescence of particles under an electron beam, RSC Adv. 2 (1) (2012) 259–263.
[38] N. Semaltianos, Nanoparticles by laser ablation, Crit. Rev. Solid State Mater. Sci. 35 (2) (2010) 105–124.
[39] D.W. Bäuerle, Laser Processing and Chemistry, Springer Science & Business Media, 2013.
[40] V. Vendamani, S. Hamad, V. Saikiran, A. Pathak, S.V. Rao, V.R.K. Kumar, S.N. Rao, Synthesis of ultra-small silicon nanoparticles by femtosecond laser ablation of porous silicon, J. Mater. Sci. 50 (4) (2015) 1666–1672.
[41] K. Abderrafi, R. Garcia Calzada, M.B. Gongalsky, I. Suárez, R. Abarques, V.S. Chirvony, V.Y. Timoshenko, R. Ibánez, J.P. Martínez-Pastor, Silicon nanocrystals produced by nanosecond laser ablation in an organic liquid, J. Phys. Chem. C 115 (12) (2011) 5147–5151.
[42] V. Švrček, T. Sasaki, Y. Shimizu, N. Koshizaki, Blue luminescent silicon nanocrystals prepared by ns pulsed laser ablation in water, Appl. Phys. Lett. 89 (21) (2006) 213113.
[43] S. Hamad, G. Krishna Podagatlapalli, R. Mounika, S. Nageswara Rao, A. Pathak, S. Venugopal Rao, Studies on linear, nonlinear optical and excited state dynamics of silicon nanoparticles prepared by picosecond laser ablation, AIP Adv. 5 (12) (2015) 127127.
[44] V. Balakrishnan, H.A. Ab Wab, K.A. Razak, S. Shamsuddin, In vitro evaluation of cytotoxicity of colloidal amorphous silica nanoparticles designed for drug delivery on human cell lines, J. Nanomater 2013 (2013) 1–8.
[45] I. Rahman, P. Vejayakumaran, C. Sipaut, J. Ismail, C. Chee, Size-dependent physicochemical and optical properties of silica nanoparticles, Mater. Chem. Phys. 114 (1) (2009) 328–332.
[46] R. Selvaggi, L. Tarpani, A. Santuari, S. Giovagnoli, L. Latterini, Silica nanoparticles assisted photodegradation of acridine orange in aqueous suspensions, Appl. Catal. B 168 (2015) 363–369.
[47] P. Sudeep, Z. Page, T. Emrick, Pegylated silicon nanoparticles: synthesis and characterization, Chem. Commun. 46 (2008) 6126–6127.
[48] P. Shen, N. Uesawa, S. Inasawa, Y. Yamaguchi, Stable and color-tunable fluorescence from silicon nanoparticles formed by single-step plasma assisted decomposition of SiBr4, J. Mater. Chem. 20 (9) (2010) 1669–1675.
[49] S. Hamad, G.K. Podagatlapalli, V. Vendamani, S. Nageswara Rao, A. Pathak, S.P. Tewari, S. Venugopal Rao, Femtosecond ablation of silicon in acetone: tunable photoluminescence from generated nanoparticles and fabrication of surface nanostructures, J. Phys. Chem. C 118 (13) (2014) 7139–7151.
[50] D. Alima, Y. Estrin, D.H. Rich, I. Bar, The structural and optical properties of supercontinuum emitting Si nanocrystals prepared by laser ablation in water, J. Appl. Phys. 112 (11) (2012) 114312.
[51] M. Wolkin, J. Jorne, P. Fauchet, G. Allan, C. Delerue, Electronic states and luminescence in porous silicon quantum dots: the role of oxygen, Phys. Rev. Lett. 82 (1) (1999) 197.
[52] S. Yang, W. Cai, H. Zhang, X. Xu, H. Zeng, Size and structure control of si nanoparticles by laser ablation in different liquid media and further centrifugation classification, J. Phys. Chem. C 113 (44) (2009) 19091–19095.
[53] S. Yang, W. Li, B. Cao, H. Zeng, W. Cai, Origin of blue emission from silicon nanoparticles: direct transition and interface recombination, J. Phys. Chem. C 115 (43) (2011) 21056–21062.
[54] V. Svrcek, D. Mariotti, T. Nagai, Y. Shibata, I. Turkevych, M. Kondo, Photovoltaic applications of silicon nanocrystal based nanostructures induced by nanosecond laser fragmentation in liquid media, J. Phys. Chem. C 115 (12) (2011) 5084–5093.
[55] T. Uchino, N. Kurumoto, N. Sagawa, Structure and formation mechanism of blue-light-emitting centers in silicon and silica-based nanostructured materials, Phys. Rev. B 73 (23) (2006) 233203.
[56] H. Tamura, M. Rückschloss, T. Wirschem, S. Vepřek, Origin of the green/blue luminescence from nanocrystalline silicon, Appl. Phys. Lett. 65 (12) (1994) 1537–1539.
[57] J.M. Hollas, Modern Spectroscopy, John Wiley & Sons, 2004.
[58] H. Desarkar, P. Kumbhakar, A. Mitra, Effect of ablation time and laser fluence on the optical properties of copper nano colloids prepared by laser ablation technique, Appl. Nanosci. 2 (3) (2012) 285–291.
[59] M.I. Mendivil Palma, B. Krishnan, G.A.C. Rodriguez, T.K. Das Roy, D.A. Avellaneda, S. Shaji, Synthesis and properties of platinum nanoparticles by pulsed laser ablation in liquid, J. Nanomater 2016 (2016) 1–11.
[60] R. Intartaglia, K. Bagga, M. Scotto, A. Diaspro, F. Brandi, Luminescent silicon nanoparticles prepared \by ultra short pulsed laser ablation in liquid for imaging applications, Opt. Mater. Express 2 (5) (2012) 510–518.
[61] K. Sasaki, N. Takada, Liquid-phase laser ablation, Pure Appl. Chem. 82 (6) (2010) 1317–1327.

View publication stats